An operationally broadened alkaline water electrolyser enabled by highly stable poly(oxindole biphenylene) ion-solvating membranes

Xu Hu
Institute of Coal Chemistry, Chinese Academy of Sciences
Bin Hu
Institute of Coal Chemistry, Chinese Academy of Sciences
Min Liu
Institute of Coal Chemistry, Chinese Academy of Sciences
Huabing Tao
Xiamen University
Yingda Huang
Institute of Coal Chemistry, Chinese Academy of Sciences
Shuanyan Kang
Institute of Coal Chemistry, Chinese Academy of Sciences
Kang Geng
Institute of Coal Chemistry, Chinese Academy of Sciences
Nanwen Li (linanwen@sxicc.ac.cn)
Institute of Coal Chemistry, Chinese Academy of Sciences https://orcid.org/0000-0002-2191-8123

Article

Keywords:

Posted Date: October 24th, 2022

DOI: https://doi.org/10.21203/rs.3.rs-2163104/v1

Additional Declarations: There is **NO** Competing Interest. The authors declare no competing interests.

Version of Record: A version of this preprint was published at Nature Energy on January 15th, 2024. See the published version at https://doi.org/10.1038/s41560-023-01447-w.

Abstract

Advanced water electrolysers represent a new direction in the field of low-cost green hydrogen production. However, the high cost of precious metal-catalysts in proton-exchange-membranes electrolysers, the high gas permeation of porous diaphragms and the alkaline instability at elevated temperatures (< 60°C) of anion-exchange-membranes in alkaline electrolysers remarkably limit their operational flexibility. Here, we demonstrate a different class of alkaline-water-electrolyser based on highly-stable oxindole/KOH complex ion pairs in poly(oxindole biphenylene) ion-solvating-membranes that can bridge the gap in existing water electrolysis technologies by enabling the use of non-precious metal-catalysts (Ni, Ni/Fe) and broadening operation temperature range (-35 ~ 120°C), in combination with ultralow gas permeation and thus low-transient-response times (< 1 s). These ISMs exhibit inspiring alkaline stability at 80°C with a negligible conductivity decay of more than 15000 h and thus allow durable alkaline electrolysis over 2500 h even at elevated temperatures and high operating voltages of 2.3 V.

Introduction

Water electrolysis to produce green hydrogen represents a key technology for renewable energy, which is essential for the decarbonization of the transportation and industrial sectors[1–4]. This process efficiently stores electricity from renewable energy sources in chemical bonds in the form of high-purity hydrogen[3,5,6]. Traditional alkaline electrolysers with a circulating alkaline solution (30–40 wt % KOH) and a porous diaphragm have the primary advantage of allowing utilization of inexpensive non-platinum metal (PGM) catalysts (such as Ni foam) under alkaline conditions[2,7,8]. However, the porous diaphragms in alkaline water electrolysers (AWEs) result in high gas permeation between the anode and cathode and blow-out of the electrolyte. As a result, these systems are no effective at elevated current densities (< 500 mA/cm^2) and display a high transient response time to maintain balanced pressure, making them unsuitable for renewable energy source applications[3,6].

Thus, polymeric electrolyte membranes (such as proton exchange membranes (PEMs) and anion exchange membranes (AEMs)) have been developed to replace porous diaphragms with liquid electrolytes[9–13]. In this case, the dense PEMs or AEMs shows excellent gas barrier ability, e.g. much lower gas permeation. Thus, the use of dense membranes in water electrolysis allows the design of a compact system with durable/resistant structural properties at high differential pressures and rapid transient response times that is adaptable to the fluctuation of renewable energy sources such as wind and solar energy. Although the PEMs electrolyser systems feature promising advantages due to the high stability and durability of perfluorosulfonic acid (PFSA) membranes, their disadvantages of distance lie in their high capital cost resulting from their use of high loading of precious platinum and iridium catalysts (IrO_2), as well as precious metal-coated titanium porous transport layers and bipolar plates[5,12]. In contrast, the AEMs electrolyser based on a polymer with fixed cationic side groups[3,14–17] shows the advantages of a low-cost PGM-free catalyst as well as low gas permeation; however, the insufficient alkaline stability of AEMs (< 5000 h) and device durability at elevated temperatures above 60°C due to SN2 substitution[6] and

Hoffman elimination[11] of fixed cationic groups and free radical attack[18] in an electrochemical environment remain crucial challenges for AWE applications.

Thus, an operationally flexible polymer electrolyte membrane with high alkaline and device stability at elevated temperatures (≥ 80°C), and good hydroxide conduction is desired to bridge the gap in these water electrolysis technologies by enabling a wide range of active, non-precious metal catalysts, in combination with ultralow gas permeation and thus low transient response times[2,19]. When a polymer is used as a membrane under alkaline water electrolysis, the fixed cationic groups may substantially limit the stability, given that the alkaline-doped polybenzimidazole[20] and ZrO_2/PSf membranes[8] without fixed ionic groups are much more stable than the sulfonated/quaternized hydrocarbon polymers. Owing to the highly ionic conduction of liquid KOH electrolytes, fixed cationic groups for intrinsic hydroxide conduction in alkaline membranes are not an essential requirement. In contrast, functional groups in the polymer that be imbibed with KOH to form a homogeneous ternary electrolyte system of polymer/water/KOH are desired. Ion solvating membranes (ISMs)[8,21,22] utilize the uptake and presence of an aqueous alkaline electrolyte to achieve ionic conductivity. Thus, the KOH-doping of a weak-base polymer, such as polybenzimidazole (PBI), was first demonstrated as an ISM[23] and exhibits promising alkaline stability for up to 2000–5000 hours, which is much longer than that of an AEM with a fixed cationic group[22–26]. An assembled alkaline electrolyser with optimized RANEY@-type electrodes achieved an impressive performance of 1.7 A cm^{-2} at 1.8 V and a wide operating current density[8]. Nevertheless, notable degradation by the ring-opening of deprotonated benzimidazole moieties in the cell potential and eventual cell failure were also observed during long term tests when the operation temperature was more than 60°C[8,9,22,26,27]. Thus, achieving long operating durability using non-precious metal catalysts over a broader range of operation temperatures in an alkaline environment has become a critical challenge for operationally flexible polymer electrolyte membrane water electrolysers.

In this work, we demonstrate that AWEs based on novel and highly stable oxindole/KOH complex ion pairs in poly(oxindole biphenylene)(POBP) ISMs can avoid the limitations of traditional AWEs, PEMs, and AEMs water electrolysis, enabling operation under a wide range of operating conditions that are not accessible with existing electrolysis technology. This ISM can conduct ions through stable oxindole/KOH complex ion pairs and enable AWE operation using a non-precious metal catalyst of Ni foam or Ni/Fe with a long durability over a broad temperature range from − 35 to 120°C and ultralow gas permeation and thus transient response times (< 1 s).

Results And Discussion

LUMO energy and alkaline stability of deprotonated oxindole/KOH complex ion pairs

The operation durability of ISMs in AWEs at an elevated temperature is dictated by the lowest unoccupied molecular orbital (LUMO) energy of the deprotonated base moieties (for example, benzimidazole) in

water. The highest occupied molecular orbital (HOMO) energy of OH^- (in water) determined via density functional theory (DFT) calculation[28] was found to be − 3.068 eV, which is lower than the LUMO energy of deprotonated benzimidazole anions. Thus, the nucleophilic attack of OH^- could be restricted by the LUMO energy of deprotonated benzimidazole anions. As a result, a higher LUMO energy will make it more difficult for deprotonated benzimidazole anions to be attacked by OH^- anions. As shown in Fig. 1a, the deprotonated benzimidazole has a LUMO energy of − 1.450 eV, which is 1.618 eV greater than that of the HOMO energy of OH^-. However, the LUMO energies of the deprotonated weak base oxindole and 3,3-diphenylhydroxindole in water were calculated to have be -0.692 eV and − 1.125 eV, respectively. These values are greater than those of the deprotonated benzimidazole anion, indicating the difficulty of attack by hydroxide ions and thus the potentially high alkaline stability. To further confirm the alkaline stability of the deprotonated oxindole anion, the model compound of 3,3-diphenyloxindole was designed and synthesized by the superacid catalysed Friedel-Crafts reactions[29]. Subsequently, the alkaline stability of this model compound was determined in 8 M KOH at 80°C. As expected, no obvious degradation was observed after 700 h of stability testing, as determined by ^{13}C NMR and ^{1}H NMR spectroscopies (Fig. 1b and Supplementary Fig. 1). In contrast, benzimidazole displayed degradation by the ring-opening reaction of imidazole groups after only 700 h under the same testing conditions (Supplementary Fig. 2 and Fig. 3).

Poly(oxindole biphenylene) (POBP) synthesis, membrane preparation and characterization

Subsequently, as shown in Fig. 2a, oxindole was successfully introduced into the aryl-ether-free polymer by superacid-catalysed polymerization of biphenyl and isatin with a batch size of more than 60 g per batch to produce poly(oxindole biphenylene) (POBP)[30,31]. ^{1}H NMR analysis confirmed the polymer structure[30], as shown in Fig. 2b. Despite the rigid polymer backbone of POBP, as confirmed by the high Tg of over 500°C (Supplementary Fig. 4), high molecular weights were obtained (M_w > 60000 Da), and the polymer displayed excellent solubility in common solvents, such as DMSO, NMP, DMF and DMAc (Supplementary Table 2). An intrinsic viscosity in DMF of 2.20 dL/g was achieved, which satisfies the requirement of large-area thin and transparent membrane preparation (Fig. 2b).

The POBP polymer was dissolved into DMF to obtain a solution and then decanted into a casting dish. After evaporating the solvent, a tough, flexible and transparent membrane was obtained. Subsequently, the POBP membrane was submerged in aqueous KOH to obtain an ion-conductive ISM (Fig. 2a). The ternary electrolyte system (POBP/H_2O/KOH) composition of the ISM was used to evaluate the concentration of KOH in the ISM, which would have a significant influence on the ionic conductivity. Generally, a high concentration of KOH electrolyte leads to a high KOH concentration in ISMs. Thus, as shown in Fig. 2c, the concentration of KOH in the POBP/H_2O/KOH system increased from 6.31–18.46% when the KOH electrolyte increased from 1 M to 8 M. However, these values were slightly lower than those of the mPBI membrane, ranging from 7.66 to 20.43% under the same testing conditions. The lower KOH absorption of the POBP membrane could be attributed to its high pKa value of 18.5 (Supplementary Fig. 5), which makes the Bronsted acid-base reaction to deprotonate between oxindole and KOH difficult.

In addition to the KOH concentration in the membrane, the water concentration also plays an important role in ionic conductivity[32]. The water uptake of the membrane increased from 10.13–23%, while that of KOH increased from 6.31–13.45% when the KOH electrolyte increased from 1 M to 6 M, respectively (Fig. 2c). The water uptake of the membrane decreased when the concentration of KOH electrolyte increased to 8 M despite its increased KOH concentration. Thus, the POBP membrane doped with 6 M KOH displayed the lowest contact angle of 21.1°, e.g., the highest wettability (Supplementary Fig. 6). It is believed that excessive KOH concentration will result in a decrease in-water held in the polymer matrix due to a concentrating effect of the polymer phase with respect to water in the higher KOH concentration regime and extensive crystallization of the polymer matrix[22], as evidenced by the gravimetric (Fig. 2c) and latter XRD results. The results of the composition and hydrophilicity of the membranes initially suggested that the optimum concentration of KOH for the POBP-ISMs is 6 M, which was fully verified by the subsequent conductivity analysis. Then the swelling behaviour of the membrane was studied at 0–6 M. Generally, high water uptake and KOH absorption lead to a high swelling ratio of the membranes. As shown in Supplementary Fig. 7, anisotropic swelling behaviour was observed with the highest dimensional swelling at 6 M KOH. The increased dimensional swelling with KOH concentration could be explained by higher water/KOH uptake. As confirmed by the XRD results shown in supplementary Figs. 8–9, the corresponding d-spacing increased from 3.76 to 4.16 Å when the swelling ratio increased, indicating that the swelling of complete protonation of the POBP due to the extensive higher KOH uptake resulted in a loosening of polymer chain packing.

To confirm the chemical structures of KOH-doped POBP-ISMs, ^{1}H NMR spectroscopy and XPS were carried out. As shown in supplementary Fig. 10, the disappearance of the N-H proton peak in the isatin spectrum at ~ 10.85 ppm implies the deprotonation of N-H in the oxindole moieties after equilibration in aqueous bulk KOH solution[22,32]. Moreover, the appearance of new peaks at 377.5, 292.5, 33.5, and 16.3 eV, which were ascribed to K 2s, K 2p, K 3s, and K 3p, further confirms the K^{+} doping of the POBP membrane[32] (Supplementary Fig. 11).The negative shifts of the N 1s and O 1s spectra of POBP and the appearance of new peaks assigned to N-K and O-K suggested that K^{+} is bonded to the deprotonated oxindole group by an acid-base reaction (Supplementary Fig. 12 and Fig. 13)[32,33]. In addition to the KOH/oxindole ion pairs, a large amount of free KOH was also absorbed in the membrane, as confirmed by the KOH peaks in the XPS spectra (Supplementary Fig. 11), consistent with the XRD results, which can induce the excellent hydroxide conduction of POBP ISM in the KOH solution.

POBP membrane also displayed excellent mechanical properties, with a stress of 75.5 MPa and a strain at break of 9.3% under 30% RH at room temperature (Fig. 2d). More interestingly, the KOH-doped POBP membrane demonstrated negligible stress loss but an increased strain at a break of 31% after KOH doping even at a high KOH concentration of 6 M. Although KOH doping decreased the thermal stability, the KOH-doped POBP membrane, even at a high KOH concentration of 6 M, showed a first onset decomposition temperature as high as 250°C (Supplementary Fig. 14), suggesting its excellent thermal stability as an ISM in AWE applications. Furthermore, the gas permeability is another important property for ISMs used in AWEs, as it determines not only the Faradaic efficiency but also the safety of

operation[26,34]. Considering that there is currently no satisfactory ex situ method to measure the hydrogen permeability of membranes in contact with KOH solutions, we tested the gas permeability of membranes in a dry state at 35°C using a homemade pure-gas permeability testing system by the volume-constant method. As shown in Fig. 2e, the gas permeability of the pristine POBP membranes was found to be 17.8 barrer for H_2 and 1.8 barrer for O_2 at 35°C (1 barrer = 10^{-10} cm^3 (STP) cm $cm^{-2}s^{-1}$ $cmHg^{-1}$). However, after doping with KOH, the gas permeabilities of the POBP membranes decreased significantly with increasing KOH concentration. The KOH-doped POBP membrane in 6 M KOH showed a H_2 permeability of 6.2 barrer and an O_2 permeability of 0.2 barrer. These values are much lower than those of Nafion@, the prototypical PEM used in existing commercial PEMs water electrolysis, indicating promising application in AWEs as membranes at elevated operation pressures (Fig. 2e).

Ionic conductivity

As shown in Fig. 3a, the ion conductivity in the through-plane direction of the POBP membrane was recorded as a function of KOH concentration and temperature. As expected, the conductivity of the membrane increased with KOH concentration because of the presence of more sites for ion transportation with a higher-concentration KOH-doped POBP membrane. Moreover, the enhancement of water movement and ion migration induced higher ionic conductivity at elevated temperatures, as shown in Fig. 3a. The highest ionic conductivity of 86.72 mS/cm was achieved when the POBP membrane was doped with 6 M KOH at 90 °C. Although this value is lower than that of the mPBI membrane because of its lower degree of KOH doping under the same testing conditions, it is high enough for this material to serve as an ISM for AWEs. Upon further increasing the concentration of KOH to 8 M, the lower ionic conductivity of the POBP membrane decreased, probably due to its lower water uptake, as discussed above. Moreover, Arrhenius behaviour as a function of temperature was also observed for all of the KOH-doped POBP membranes (Supplementary Fig. 15). The activation energies for ion conduction of the aqueous KOH solutions were calculated to be in the range of 16.56–24.25 kJ/mol based on the slope of ln (σ) vs. 1/T using the Arrhenius equation and tended to obviously increase with increasing KOH concentration, indicating the occurrence of the Grotthuss mechanism of ion transport[32] in the POBP ISMs.

Alkaline and oxidative stability

Membrane stabilities, including alkaline and oxidative stabilities, which are crucially important for the practical operation of these membranes in AWEs, were comprehensively evaluated. Impressively, the aryl ether-free polyaromatics showed robust alkaline stability even under harsh conditions of 8 M KOH at 80°C. No appreciable change in ionic conductivity (Fig. 3b) was observed even over a long test period of 15,000 h (> 600 days) which is much longer than the stability of the ISM based on the PBI polymers and previously reported AEMs[3,8,16,17,22,24]. Moreover, as shown in Fig. 3d, no detectable change in the chemical shift in the ^1H NMR spectra was observed, further demonstrating the excellent alkaline stability of the polymer backbone and functional groups of oxindole. These results were further confirmed by model compound stability testing, as discussed above. Therefore, it is remarkable that the POBP ISM

shows competitive alkaline stability and reasonable ion conductivity, which have seldom been achieved simultaneously in previous reports.

The oxidative stability with respect to weight was investigated by immersing membranes in Fenton reagent (3 wt% H_2O_2 with 4 ppm $FeSO_4$) at 80°C[35], in which hydroxyl (·OH) and hydroperoxy (·OOH) radicals were produced from the decomposition of H_2O_2 catalysed by Fe^{2+}. As shown in Fig. 3c, the mPBI membrane showed a poor oxidative stability, e.g., breaking into pieces, with a steep weight decline of approximately 35 wt% within only 300 h. A possible degradation mechanism was confirmed by analysis of aged mPBI membranes using the FT-IR technique due to the insolubility of this material (Supplementary Fig. 16). As shown in Supplementary Fig. 17, the appearance of new stretching vibration peaks at 1801 cm^{-1} attributed to the C = O group, 1690 cm^{-1} attributed to aromatic ketones, and 1568–1572 cm^{-1} attributed to -NO_2 suggests a ring-opening mechanism[32,36,37] to form carboxylic acid derivatives and nitro groups (Supplementary Fig. 18). In contrast, the POBP ISM exhibited impressive oxidative stability under the same testing conditions. It remained intact and flexible even after over 1000 h, with a weight loss of less than 11 wt%. This weight loss of the POBP ISM was confirmed to be caused by a decrease in the thickness of ~ 11%, indicating the occurrence of reasonable surface oxidative degradation of the membrane. More importantly, no obvious changes were observed in the mechanical properties or chemical structures of aged POBP membrane, as confirmed by the FT-IR and NMR spectra (Fig. 3d and Supplementary Figs. 19–20). This excellent oxidative stability was attributed to the aryl ether-free polymer backbone[6,16,34] and the lower water uptake of POBP (~ 7 wt%) in which water was an effective catalyst for radicals to attack the hydrogen–carbon polymer backbone[18,37].

Awe Device Performance And Durability

To demonstrate the device performance of POBP ISMs, an AWE was designed (supplementary Fig. 21) and applied at 80°C in a 6 M aqueous KOH solution using naked Ni-foam as a catalyst both in the anode and cathode due to its high stability despite its the lower activity. As shown in Fig. 4a, the POBP ISM exhibited better performance than the state-of-the-art PPS and Zirfon® diaphragms in both the kinetic and mass-transport-controlled regions. The superior performance of the POBP ISM was attributed to its relatively low high-frequency resistance (HFR) of as low as ~ 0.203 Ω cm^2 at 125 mA/cm^2 and 80 °C in 6 M KOH. This value is significantly lower than those of PPS (0.402 Ω cm^2) and the Zirfon® diaphragm (0.287 Ω cm^2). Moreover, the superior performance in the kinetic region suggested that the ISM resistance had a significant effect on the catalyst activity in the electrolyser. Thus, the inclusion of a highly active catalyst is believed to be an effective approach to further improve water electrolysis performance. As expected, as shown in Fig. 4b, the NiFe-anode-catalysed electrolyser using POBP ISMs and a Pt/C cathode outperformed the AWEs with a naked Ni-foam or Ni/Al alloy catalyst in both the kinetic and mass-transport-controlled regions. The optimized electrolyser with a NiFe-anode-catalyst in 6 M KOH at 80°C showed a 2.0 A/cm^2 at 1.9 V, which is comparable to that of the state-of-the-art Nafion

115® in a PEM electrolyser and almost 5 times higher than that of traditional AWEs based on Ni-form or Ni/Al alloy catalysts (~ 0.4–0.5 A/cm^2 at 1.9 V).

We further investigated the performance of the POBP ISMs in various concentrations of KOH. In the kinetic region, the ISMs exhibited similar performance because they used the same catalyst, suggesting the negligible effect of the KOH concentration on the Ni-foam catalyst activity (Supplementary Fig. 22). However, in the mass-transport-controlled region, a high KOH concentration induced better performance, probably due to the high ion conductivity (Fig. 3a) and low resistance of the ISMs (Supplementary Fig. 23). Thus, because of the remarkable dependence of ion conductivity and area resistance (AR) on the temperature (Fig. 4c), the operation temperature of the electrolyser exerted a significant influence on the electrolyser performance. As shown in Fig. 3a, high temperature resulted in high conductivity and thus high electrolyser performance, particularly in the mass-transport-controlled region. Surprisingly, the ISM-based electrolyser without any external heating system easily started at temperatures as low as -35°C with an ultralow starting time of less than 1 s even after a freezing time of 60 h (Supplementary Figs. 24–26), which is unattainable for the PEM or AEM AWEs due to the freezing of pure water. Compared to state-of-the-art porous PPS and Zirfon® diaphragms, AWEs based on dense POBP ISMs showed significant enhancements in transient response times of 1700 ~ 2700 times at -35°C (Supplementary Fig. 27), which is believed to contribute to the lower area resistance of the POBP membrane even at an ultralow temperature of -35°C (Fig. 4c and Supplementary Fig. 28a).

Moreover, as shown in Fig. 4d and Supplementary Fig. 28b, a reasonable electrolyser performance was observed at an operating temperature of 120°C, indicating operability at high temperatures, although it is lower than that of the ISMs at 80°C, probably due to the lower water uptake at temperatures greater than the water boiling point, which would lead to increasing area resistance (Fig. 4c). Similar to the ultralow-temperature operability, operation of the PEMs and AEMs electrolysers at high temperatures over 80°C is also unattainable due to the lower Tg of Nafion®[12] and the low alkaline stability of the AEMs[6,11], respectively. Therefore, the POBP ISM-based alkaline electrolyser has been demonstrated to be one of the broadest water electrolysis operation temperature ranges achieved thus far, and can operate smoothly from − 35 to 120°C.

The high alkaline and oxidative stabilities of the polymer electrolyte membrane are believed to induce high electrolyser device durability. At 80°C, the in situ durability of a POBP ion-solvating membrane was investigated using 6 M KOH alkaline electrolysers with Ni-foam as a catalyst. Impressively, the cell voltage remained steady at a voltage as high as 2.3 V for over 2500 h at a current density of 500 mA cm^{-2}, as shown in Fig. 5a. This superior cell durability was much better than that of the mPBI ISM, which shows an obvious cell performance decay after only 130 hours under the same testing conditions. The ring-opening degradation mechanism of benzimidazole moieties in mPBI was confirmed by ^{1}H NMR and FT-IR techniques (Supplementary Fig. 18 and Supplementary Figs. 29–30). In contrast, after 2500 h of cell durability testing, the POBP ISM still showed good solubility and retained its original chemical structure, as shown in Supplementary Figs. 31–32. No appreciable new peak and/or chemical shifts of

protons were observed in the ^{1}H NMR and FT-IR spectra, suggesting one of the longest stability of alkaline electrolysers under harsh operational environments at a high voltage (~ 2.3 V), a high temperature (80°C) and a high KOH concentration (Fig. 5b and Supplementary Fig. 33). Combined with these high stabilities and durability, the use of a non-precious metal catalyst, broad operation temperature range, broad KOH concentration range and low gas permeation of the ISM, an operationally flexible AWE with a POBP ISM was successfully achieved.

Conclusions

In summary, we established highly stable oxindole/KOH complex ion pairs in POBP-ISMs for AWEs. The high LUMO energy of deprotonated oxindole anions was confirmed by DFT calculations and induced an exciting alkaline stability of the POBP membrane without appreciable conductivity loss over 15000 h in 8 M KOH at 80°C. The aryl-ether-free polymer backbone and lower water uptake of the POBP membrane further resulted in excellent oxidative stability in a Fenton reagent (> 1000 h at 80°C). Thus, this highly stable ISM can bridge the existing gap in water electrolysis technologies under flexible operation conditions by enabling a non-precious metal catalyst, low gas permeation, a broadened operation temperature range and long operation durability. An unoptimized POBP-ISM AWE with a nickel-foam electrode was applied successfully over a broad operating temperature window (-35 ~ 120°C) with a rapid start-up (< 1 s) even at a low temperature of -35°C. High performance with an operating current density of 2.0 A/cm^2 at 1.9 V was achieved when the Ni/Fe catalyst was utilized in an anode that was comparable with that of an IrO_2-anode-catalysed PEMs electrolyser. This operational flexibility of ISM AWEs over a wide range of temperatures, a non-precious metal catalyst, low transient response times and long durability, which is unattainable with existing water electrolysis technology, could enable the simplification and cost reduction of electrolyser systems for green hydrogen production applications.

Methods

Materials. Biphenyl (99%), trifluoromethanesulfonic acid (TFSA, 99%), trifluoroacetic acid (TFA, 99%), benzene (99%), 2-phenylbenzimidazole (99%) and isatin (98%) were obtained from Energy Chemical. Dichloromethane (DCM, 99.5%), *N,N*-dimethylformamide (DMF), dimethyl sulfoxide (DMSO), *N*-methyl-2-pyrrolidone (NMP), *N,N*-dimethylacetamide (DMAc), ethanol (99.7%) and potassium carbonate (K_2CO_3) were purchased from Sinopharm Chemical Reagent Factory and used as received. Aqueous solutions of KOH with concentrations of 1, 2, 4, 6 and 8 mol L^{-1} were prepared by dissolving Potassium hydroxide pellets (Macklin, GR) in deionized (DI) water.

Synthesis of 3,3-diphenyloxindole and POBP. 3,3-Diphenyloxindole was obtained by mixing an excess of benzene (10 mL, 0.113 mol) and isatin (1.66 g, 11.3 mmol) with TFSA (10 equiv.) at 0°C overnight. For the production of the high-molecular-weight POBP polymer, isatin (32 g, 21.8 mmol), biphenyl (30 g, 19.4 mmol), and hydrous DCM were typically combined in a 500 ml round-bottom flask. Trifluoroacetic acid (TFA, 34.0 mL) and trifluoromethanesulfonic acid (TFSA, 126.0 mL) were added dropwise at 0°C. The

reaction mixture was then agitated at 0°C for an additional 8 hours and then placed into an aqueous ethanol solution and 1 M K_2CO_3 to remove the residual acid. Finally, with a 99% yield, the white fibrous product was filtered, rinsed with DI water, and dried overnight in a vacuum oven at 80°C. The intrinsic viscosity of POBP was determined to be η_{int} = 2.20 dL g^{-1} in DMF at 30°C. ^{1}H NMR (400 MHz, DMSO-d_6, ppm) δ: 10.85 (s, 1H), 7.58 (s, 4H), 7.25 (s, 6H) and 6.99 (s, 2H).

Characterizations of structure. ^{1}H NMR and ^{13}C NMR spectroscopy was performed by using a Bruker DPX-400 instrument with DMSO-d_6 and tetramethylsilane (TMS) as the solvents and the internal reference, respectively. The Fourier transform infrared (FT-IR) spectra were recorded on a Perkin Elmer Spectrum Two in attenuated total reflectance (ATR) mode. X-ray photoelectron spectroscopy (XPS) was performed on a Physical Electronics PHI5600 with an X-ray source operated at 12 kV and 350 W. X-ray diffraction (XRD) was carried out using a D8 ADVANCE A25 equipped with a Cu Kα source (λ = 1.54184 Å) in the range of 5–50° 2θ at a scan speed of 4°/2θ per minute and a step size of 0.02°/2θ. The *d*-spacing for the amorphous or crystalline peak maxima was calculated according to the Bragg equation.

Membrane preparation. The solution (filtered 8 wt% POBP in DMF) was cast in a clean glass dish at 80°C for at least 24 h in an oven. After immersing the glass in deionized water, the membrane was pulled off and left until it disengaged from the glass. POBP ion-solvating membranes were obtained by immersing the membrane in aqueous KOH with concentrations ranging from 0 to 8 M at 80°C for at least a week. The thickness of the obtained membrane was 45 ± 5 μm.

Characterization of the POBP ISMs. The hydrophilicity of the membranes after doping in different aqueous KOH concentrations ranging from 0 to 8 M was determined from the contact angle, using DI water on the surface of membranes. The KOH content and water content of the ISMs were determined gravimetrically using the method described by previous works [22,53]. The weight fractions of POBP (W_p), water (W_w) and KOH equivalents (W_{KOH}) were calculated as:

$$W_p = \frac{m_{dedoped}}{m} \times 100\%$$

$$W_w = \frac{(m - m_{dry})}{m} \times 100\%$$

$$W_{KOH} = \frac{(m_{dry} - m_{dedoped})}{m} \times 100\%$$

where m is the weight of membrane samples after being carefully wiped off with tissue paper, m_{dry} is the weight of samples after drying at 120°C for 12 h in a vacuum and $m_{dedoped}$ is the weight of sampled membrane after extensive washing in DI water until neutral pH followed by drying at 120°C for 12 h. The swelling ratio (SR) in the surface area and thickness of the membranes were recorded to determine the swelling characteristics on the dried membrane basis. The SR of the membranes was calculated as:

$$SR_T = \frac{T_{wet}\text{-}T_{dry}}{T_{dry}} \times 100\backslash\%$$

$$SR_A = \frac{A_{wet}\text{-}A_{dry}}{A_{dry}} \times 100\backslash\%$$

where T_{dry} and A_{dry} are the thickness and surface area of the dried membranes before doping and T_{wet} and A_{wet} are the thickness and surface area of hydrated membranes, respectively. The pure gas permeation properties of membranes were evaluated by a constant-volume/variable-pressure method (constant downstream volume permeation apparatus)[54]. Before testing, each membrane was degassed for 24 h. Three different samples of the membranes equilibrated in aqueous bulk KOH solution were tested, and the deviation was less than 5%. Permeability (P) was calculated using the following equation:

$$P = 10^{10} \times \frac{V_d \times l}{P_{up} \times T \times R \times A} \times \frac{dp}{dt}$$

where P is the permeability (Barrer). 1 Barrer = 10^{-10} cm^3(STP) cm cm^{-2} s^{-1} $cmHg^{-1}$, V_d is the calibrated permeate volume (cm^3), l is the membrane thickness (cm), p_{up} is the upstream pressure (cmHg), A is the effective membrane area (cm^2), T is the operating temperature (K), R is the gas constant (0.278 cm^3cmHg cm^{-3}(STP) K^{-1}) and dp/dt is the steady-state downstream pressure increase rate (cmHg s^{-1}). The storage modulus and tan δ of POBP membranes were measured by a dynamic thermomechanical analysis (DMA, Q800. TA instrument, DE, USA) system. Membrane samples were cut into 9 mm × 40 mm rectangle shapes and then measured with a preload force of 0.01 N and a force track of 125% under N_2 atmosphere. The sample was ramped at 4°C min^{-1} until 460°C. The last peak of tan δ represents the glass transition temperature (Tg) of membrane sample. The mechanical properties of membrane were measured using a CMT-4502 (MTS SYSTEMS Co., Ltd., China) mechanical testing instrument at a crosshead speed of 5 mm/min at 40% RH. The thermal stability of doped membranes was investigated by thermogravimetric analysis (TGA) using a PerkinElmer TGA-7 thermogravimetric analyser at a heating rate of 10°C/min under a nitrogen atmosphere. All the membranes were dried under a vacuum oven at 110°C overnight before the analysis.

Computational details and simulation. Alkaline stability: Theoretical calculations of the 3,3-diphenyloxindole and 2-phenylbenzimidazole salt molecules were performed by Dmol embedded in the Materials Studio software system package[28]. The GGA-BLYP functional and double numerical plus polarization basis set were employed for the calculations. The single molecules are all optimized with a self-consistent field (SCF) convergence value of 10^{-6} Ha. Considering the solution surroundings, the solvent (water, ε = 78.54) impact was supplemented into the calculations.

Conductivity measurement. Through-plane conductivity of POBP after alkaline equilibration by immersion in aqueous KOH was obtained using impedance spectroscopy by impedance/gain phase analyser (Bio-Logic VSP-300, FR) over the frequency range from 50 mHz to 100 kHz according to previous

reports[22,25,26]. The separator samples with an active area of 2.0 cm^2 in the H-cell with a Pt electrode were mounted between two chambers. The interspace was filled with the corresponding KOH solution. The conductivity (σ) was calculated as:

$$\sigma = \frac{t}{A \times (R\text{-}R_{blank})}$$

The area resistance (AR) was calculated by the following equation:

$$AR = A \times (R - R_{blank})$$

where t (cm) is the thickness of the membrane, R (Ω) is the resistance of the electrodes with the membrane, the R_{blank} (Ω) is the resistance of the electrodes without the membrane and A (cm^2) represents the available cross-sectional membrane area.

Chemical stability. Alkaline stability: The POBP was evaluated in 6 and 8 M KOH at 80°C, and the variations in the membranes before and after the alkaline stability test were also analysed by FT-IR, ^1H NMR and conductivity measurements. Oxidative stability: The Fenton test (4 ppm Fe^{2+} at 3 wt% H_2O_2 at 80°C) was used to detect the weight loss and chemical changes in membranes caused by radical-induced oxidation. After a certain period, the membranes were removed, thoroughly washed with DI water, and dried at 120°C for 8 hours before testing. To continue the test, the membrane samples were placed in newly produced Fenton solutions.

Performance and durability for AWE. The alkaline water electrolyzer experiments were carried out using our homemade electrolysers[11,53]. Optimized membrane electrode assembly (MEA) preparation: A catalyst-coated-membrane (CCM) method was used to fabricate the MEA using Fe-Ni as the anode and Pt/C as the cathode. Typically, the anode catalyst was a suspension of catalyst, isopropanol, deionized water and ionomer (FAA-3). The catalyst link of the cathode was a suspension of Pt/C, isopropanol, deionized water and ionomer. Unoptimized MEA: The catalyst-coated-substrate (CCS) method was used to fabricate the MEA using nickel foam or Ni-Al electrodes as the anode and cathode. The electrolysis cell consisted of flow field plates with a linear pattern made from nickel, electrodes (9 cm^2), a membrane (4 cm^2), and gaskets (25 cm^2). Heating elements and a thermocouple were placed within the flow-field plates to control the temperature. A CT-4008-5V10A-FA instrument (NEWARE, China) controlled by a cell testing system was used for the power supply. The KOH electrolyte was actively circulated through the electrodes at 60 mL/min. The electrolyser was conditioned at 10 mA/cm^2 for 40–60 minutes to reach a steady state. The polarization curves of MEA were measured in galvanostatic mode at 10–2500 mA cm^{-2} from − 35 to 120°C. The transient-response-times: I-V curves were recorded after 0, 15, 40, and 60 hours of operation by scanning the current density at -35°C. The transient-response-time of the AWE was determined from the cell potential over the theoretical electrolytic potential, and gas was generated at the anode and cathode poles. EIS was performed in constant current density mode by means of a

multichannel Ivium electrochemical station, where the frequency was in the range of 10^5 to 0.1 Hz, and the amplitude is 100 mA.

AWE durability: The aforementioned approach using nickel foam electrodes was utilized to assess the in situ durability of the ISMs, in which the electrolyser was set to 500 mA/cm^2 (6 M KOH and 80°C). Water and electrolyte were provided manually, generally after approximately 12 hours.

Declarations

Acknowledgments

We thank X. ZHANG from Nanjing University of Science and Technology for the simulation and M. Dou at Institute of Coal Chemistry of Chinese Academy of Sciences (CAS) for the helps of NMR. The authors acknowledge the financial support for this work was provided by the National Natural Science Foundation of China (21835005 and 22105217), STS Project of Chinese Academy of Sciences (KFJ-STS-QYZD-2021-02-003), the Natural Science Foundation of Shanxi Province (No.20210302124433).

Author contributions

X. H. synthesized the polymeric materials, designed the experiments and writing-original draft. K. G. helped with data, collection formal analysis. K. G., B. H., M. L., H. T. and S. K. characterized the electrolyzer tests and review draft. Y. H., N. L. and K. G. contributed to writing the manuscript. N. L. initiated the collaborative project. K. G. and N. L. supervised and guided the work.

Competing interests

The authors declare no competing interests.

Data Availability

The data that support the plots within this paper and other findings of this study are available from the corresponding author upon reasonable request.

References

1. Pavel, C. C. *et al.* Highly efficient platinum group metal free based membrane-electrode assembly for anion exchange membrane water electrolysis. Angew. Chem. Int. Ed. Engl. **53**, 1378–1381, doi:10.1002/anie.201308099 (2014).

2. Abbasi, R. *et al.* A Roadmap to Low-Cost Hydrogen with Hydroxide Exchange Membrane Electrolyzers. Adv. Mater. **31**, e1805876, doi:10.1002/adma.201805876 (2019).
3. Li, D. *et al.* Highly quaternized polystyrene ionomers for high performance anion exchange membrane water electrolysers. Nature Energy **5**, 378–385, doi:10.1038/s41560-020-0577-x (2020).
4. Lindquist, G. A., Xu, Q., Oener, S. Z. & Boettcher, S. W. Membrane Electrolyzers for Impure-Water Splitting. Joule **4**, 2549–2561, doi:10.1016/j.joule.2020.09.020 (2020).
5. Lee, B., Lim, D., Lee, H. & Lim, H. Which water electrolysis technology is appropriate?: Critical insights of potential water electrolysis for green ammonia production. Renewable and Sustainable Energy Reviews **143**, 110963, doi:10.1016/j.rser.2021.110963 (2021).
6. Li, D. *et al.* Durability of Anion Exchange Membrane Water Electolyzers. Energy & Environmental Science **14**, 3393, doi:10.1039/d0ee04086j (2021).
7. Aili, D. *et al.* Heterogeneous anion conducting membranes based on linear and crosslinked KOH doped polybenzimidazole for alkaline water electrolysis. Journal of Membrane Science **447**, 424–432, doi:10.1016/j.memsci.2013.07.054 (2013).
8. Kraglund, M. R. *et al.* Ion-solvating membranes as a new approach towards high rate alkaline electrolyzers. Energy & Environmental Science **12**, 3313–3318, doi:10.1039/c9ee00832b (2019).
9. Thomas, O. D., Soo, K. J., Peckham, T. J., Kulkarni, M. P. & Holdcroft, S. A stable hydroxide-conducting polymer. J. Am. Chem. Soc. **134**, 10753–10756, doi:10.1021/ja303067t (2012).
10. Liu, Z. *et al.* The effect of membrane on an alkaline water electrolyzer. Int. J. Hydrogen Energy **42**, 29661–29665, doi:10.1016/j.ijhydene.2017.10.050 (2017).
11. Hu, X. *et al.* Piperidinium functionalized aryl ether-free polyaromatics as anion exchange membrane for water electrolysers: Performance and durability. Journal of Membrane Science **621**, 118964, doi:10.1016/j.memsci.2020.118964 (2021).
12. Jiao, K. *et al.* Designing the next generation of proton-exchange membrane fuel cells. Nature **595**, 361–369, doi:10.1038/s41586-021-03482-7 (2021).
13. Liu, X. *et al.* Magnetic-field-oriented mixed-valence-stabilized ferrocenium anion-exchange membranes for fuel cells. Nature Energy **7**, 329–339, doi:10.1038/s41560-022-00978-y (2022).
14. Shin, D. W., Guiver, M. D. & Lee, Y. M. Hydrocarbon-Based Polymer Electrolyte Membranes: Importance of Morphology on Ion Transport and Membrane Stability. Chem. Rev. **117**, 4759–4805, doi:10.1021/acs.chemrev.6b00586 (2017).
15. Olsson, J. S., Pham, T. H. & Jannasch, P. Poly(arylene piperidinium) Hydroxide Ion Exchange Membranes: Synthesis, Alkaline Stability, and Conductivity. Adv. Funct. Mater. **28**, 1702758, doi:10.1002/adfm.201702758 (2018).
16. Wang, J. *et al.* Poly(aryl piperidinium) membranes and ionomers for hydroxide exchange membrane fuel cells. Nature Energy **4**, 392–398, doi:10.1038/s41560-019-0372-8 (2019).
17. Chen, N. *et al.* High-performance anion exchange membrane water electrolyzers with a current density of 7.68 A cm-2 and durability of 1000 h. Energy & Environmental Science **14**, 6338–6348,

doi:10.1039/d1ee02642a (2021).

18. Holmes, T., Skalski, T. J. G., Adamski, M. & Holdcroft, S. Stability of Hydrocarbon Fuel Cell Membranes: Reaction of Hydroxyl Radicals with Sulfonated Phenylated Polyphenylenes. Chem. Mater. **31**, 1441–1449, doi:10.1021/acs.chemmater.8b05302 (2019).
19. Zhang, J. *et al.* Recent Insights on Catalyst Layers for Anion Exchange Membrane Fuel Cells. Adv Sci (Weinh), e2100284, doi:10.1002/advs.202100284 (2021).
20. Tang, H. *et al.* Fuel cells with an operational range of – 20°C to 200°C enabled by phosphoric acid-doped intrinsically ultramicroporous membranes. Nature Energy, doi:10.1038/s41560-021-00956-w (2022).
21. Merle, G., Wessling, M. & Nijmeijer, K. Anion exchange membranes for alkaline fuel cells: A review. Journal of Membrane Science **377**, 1–35, doi:10.1016/j.memsci.2011.04.043 (2011).
22. Aili, D. *et al.* Towards a stable ion-solvating polymer electrolyte for advanced alkaline water electrolysis. Journal of Materials Chemistry A **5**, 5055–5066, doi:10.1039/c6ta10680c (2017).
23. Xing B & Savadogo, O. Hydrogenroxygen polymer electrolyte membrane fuel cells (PEMFCs)based on alkaline-doped polybenzimidazole PBI. Electrochem. Commun. **2**, 697–702 (2000).
24. Aili, D., Jankova, K., Li, Q., Bjerrum, N. J. & Jensen, J. O. The stability of poly(2,2'-(m-phenylene)-5,5'-bibenzimidazole) membranes in aqueous potassium hydroxide. Journal of Membrane Science **492**, 422–429, doi:10.1016/j.memsci.2015.06.001 (2015).
25. Kraglund, M. R. *et al.* Zero-Gap Alkaline Water Electrolysis Using Ion-Solvating Polymer Electrolyte Membranes at Reduced KOH Concentrations. J. Electrochem. Soc. **163**, F3125-F3131, doi:10.1149/2.0161611jes (2016).
26. Hu, B. *et al.* A stable ion-solvating PBI electrolyte enabled by sterically bulky naphthalene for alkaline water electrolysis. Journal of Membrane Science **643**, 120042, doi:10.1016/j.memsci.2021.120042 (2022).
27. Diaz, L. A. *et al.* Alkali doped poly (2,5-benzimidazole) membrane for alkaline water electrolysis: Characterization and performance. J. Power Sources **312**, 128–136, doi:10.1016/j.jpowsour.2016.02.032 (2016).
28. Lin, B. *et al.* Alkaline Stable C2-Substituted Imidazolium-Based Anion-Exchange Membranes. Chem. Mater. **25**, 1858–1867, doi:10.1021/cm400468u (2013).
29. Klumpp, D. A., Yeung, K. Y., G. K. Surya Prakash & Olah, G. A. Preparation of 3,3-Diaryloxindoles by Superacid-Induced Condensations of Isatins and Aromatics with a Combinatorial Approach. J. Org. Chem. **63**, 4 (1998).
30. Hernandez, M. C. G. *et al.* Novel, Metal-Free, Superacid-Catalyzed “Click” Reactions of Isatins with Linear, Nonactivated, Multiring Aromatic Hydrocarbons. Macromolecules **43**, 6968–6979, doi:10.1021/ma101048z (2010).
31. Cruz, A. R. *et al.* Precision Synthesis of Narrow Polydispersity, Ultrahigh Molecular Weight Linear Aromatic Polymers by A2 + B2 Nonstoichiometric Step-Selective Polymerization. Macromolecules **45**, 6774–6780, doi:10.1021/ma301691f (2012).

32. Zeng, L., Zhao, T. S., An, L., Zhao, G. & Yan, X. H. Physicochemical properties of alkaline doped polybenzimidazole membranes for anion exchange membrane fuel cells. Journal of Membrane Science **493**, 340–348, doi:10.1016/j.memsci.2015.06.013 (2015).
33. Ye, C. *et al.* Catalytic Oxidation of K2S via Atomic Co and Pyridinic N Synergy in Potassium-Sulfur Batteries. J. Am. Chem. Soc. **143**, 16902–16907, doi:10.1021/jacs.1c06255 (2021).
34. Chen, N. *et al.* Poly(fluorenyl aryl piperidinium) membranes and ionomers for anion exchange membrane fuel cells. Nat Commun **12**, 2367, doi:10.1038/s41467-021-22612-3 (2021).
35. Yang, J. *et al.* Covalently cross-linked sulfone polybenzimidazole membranes with poly(vinylbenzyl chloride) for fuel cell applications. ChemSusChem **6**, 275–282, doi:10.1002/cssc.201200716 (2013).
36. Chang, Z., Pu, H., Wan, D., Jin, M. & Pan, H. Effects of adjacent groups of benzimidazole on antioxidation of polybenzimidazoles. Polym. Degrad. Stab. **95**, 2648–2653, doi:10.1016/j.polymdegradstab.2010.07.009 (2010).
37. Chang, Z. *et al.* Chemical oxidative degradation of Polybenzimidazole in simulated environment of fuel cells. Polym. Degrad. Stab. **94**, 1206–1212, doi:10.1016/j.polymdegradstab.2009.04.026 (2009).
38. Choe, Y.-K. *et al.* Alkaline Stability of Benzyl Trimethyl Ammonium Functionalized Polyaromatics: A Computational and Experimental Study. Chem. Mater. **26**, 5675–5682, doi:10.1021/cm502422h (2014).
39. Vengatesan, S., Santhi, S., Jeevanantham, S. & Sozhan, G. Quaternized poly (styrene-co-vinylbenzyl chloride) anion exchange membranes for alkaline water electrolysers. J. Power Sources **284**, 361–368, doi:10.1016/j.jpowsour.2015.02.118 (2015).
40. Chu, X., Shi, Y., Liu, L., Huang, Y. & Li, N. Piperidinium-functionalized anion exchange membranes and their application in alkaline fuel cells and water electrolysis. Journal of Materials Chemistry A **7**, 7717–7727, doi:10.1039/c9ta01167f (2019).
41. Li, D. *et al.* Phenyl Oxidation Impacts the Durability of Alkaline Membrane Water Electrolyzer. ACS Appl Mater Interfaces **11**, 9696–9701, doi:10.1021/acsami.9b00711 (2019).
42. Li, H. *et al.* Poly(vinyl benzyl methylpyrrolidinium) hydroxide derived anion exchange membranes for water electrolysis. Journal of Materials Chemistry A **7**, 17914–17922, doi:10.1039/c9ta04868e (2019).
43. Su, X. *et al.* Novel piperidinium functionalized anionic membrane for alkaline polymer electrolysis with excellent electrochemical properties. Journal of Membrane Science **581**, 283–292, doi:10.1016/j.memsci.2019.03.072 (2019).
44. Cha, M. S. *et al.* Poly(carbazole)-based anion-conducting materials with high performance and durability for energy conversion devices. Energy & Environmental Science **13**, 3633–3645, doi:10.1039/d0ee01842b (2020).
45. Lee, H. I. *et al.* Advanced Zirfon-type porous separator for a high-rate alkaline electrolyser operating in a dynamic mode. Journal of Membrane Science **616**, 118541, doi:10.1016/j.memsci.2020.118541 (2020).

46. Park, H. J., Lee, S. Y., Lee, T. K., Kim, H.-J. & Lee, Y. M. N3-butyl imidazolium-based anion exchange membranes blended with Poly(vinyl alcohol) for alkaline water electrolysis. Journal of Membrane Science **611**, 118355, doi:10.1016/j.memsci.2020.118355 (2020).
47. Park, Y. S. *et al.* Superior performance of anion exchange membrane water electrolyzer: ensemble of producing oxygen vacancies and controlling mass transfer resistance. Applied Catalysis B: Environmental **278**, 119276, doi:10.1016/j.apcatb.2020.119276 (2020).
48. Yan, X. *et al.* Twisted ether-free polymer based alkaline membrane for high-performance water electrolysis. J. Power Sources **480**, 228805, doi:10.1016/j.jpowsour.2020.228805 (2020).
49. Xu, Z. *et al.* Anisotropic anion exchange membranes with extremely high water uptake for water electrolysis and fuel cell. Journal of Materials Chemistry A **9**, 23485, doi:10.1039/d1ta06579c (2021).
50. Liu, M., Hu, X., Hu, B., Liu, L. & Li, N. Soluble poly(aryl piperidinium) with extended aromatic segments as anion exchange membranes for alkaline fuel cells and water electrolysis. Journal of Membrane Science **642**, 119966, doi:10.1016/j.memsci.2021.119966 (2022).
51. Diaz, L. A. *et al.* Alkali-doped polyvinyl alcohol – Polybenzimidazole membranes for alkaline water electrolysis. Journal of Membrane Science **535**, 45–55, doi:10.1016/j.memsci.2017.04.021 (2017).
52. Konovalova, A. *et al.* Blend membranes of polybenzimidazole and an anion exchange ionomer (FAA3) for alkaline water electrolysis: Improved alkaline stability and conductivity. Journal of Membrane Science **564**, 653–662, doi:10.1016/j.memsci.2018.07.074 (2018).
53. Hu, X., Liu, M., Huang, Y., Liu, L. & Li, N. Sulfonate-functionalized polybenzimidazole as ion-solvating membrane toward high-performance alkaline water electrolysis. Journal of Membrane Science **663**, 121005, doi:10.1016/j.memsci.2022.121005 (2022).
54. Chen, X. *et al.* Tailoring the Microporosity of Polymer of Intrinsic Microporosity for Advanced Gas Separation by Atomic Layer Deposition. Angew. Chem. Int. Ed. **133**, 1–7, doi:10.1002/anie.202016901 (2021).

Figures

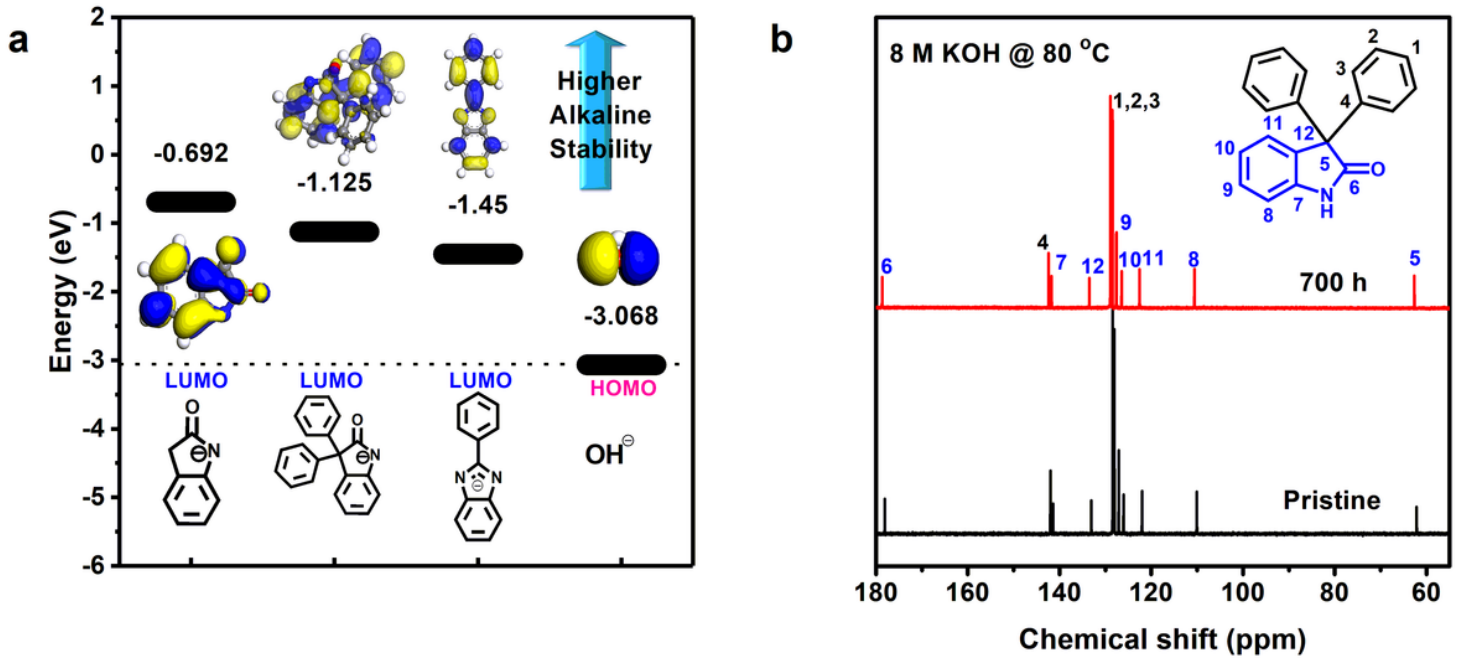

Figure 1

DFT calculation and alkaline stability test of model compounds. a, The calculated LUMO energies and isosurfaces of deprotonated model compounds and HOMO energy of OH^-; higher the LUMO energy, higher the alkaline stability of the molecule. **b,** Alkaline stability of 3,3-diphenylhydroxyindole in 8M KOH at 80 °C.

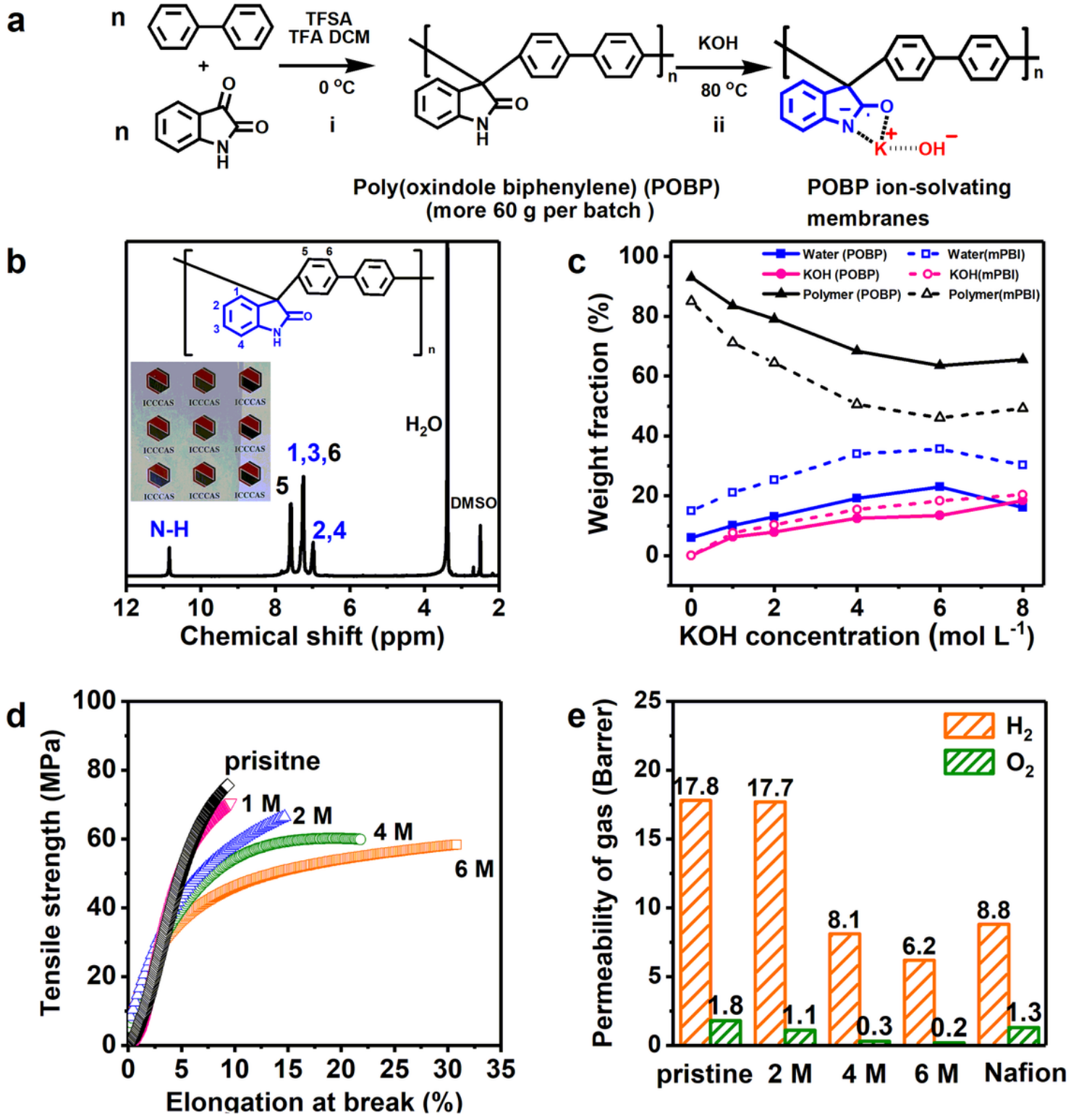

Figure 2

Preparation and characterization of POBP-ISMs. a, Synthesis of the POBP-based ion-solvating membrane (POBP-ISMs). **b,** ^{1}H NMR spectra and photograph of POBP membrane form a batch size of more than 60 g per batch. **c,** Composition with respect to the total weight. **d,** Mechanical properties of POBP-ISMs as a function of KOH concentration. **e,** Gas permeability of POBP-ISMs as a function of KOH concentration in the form of dry state.

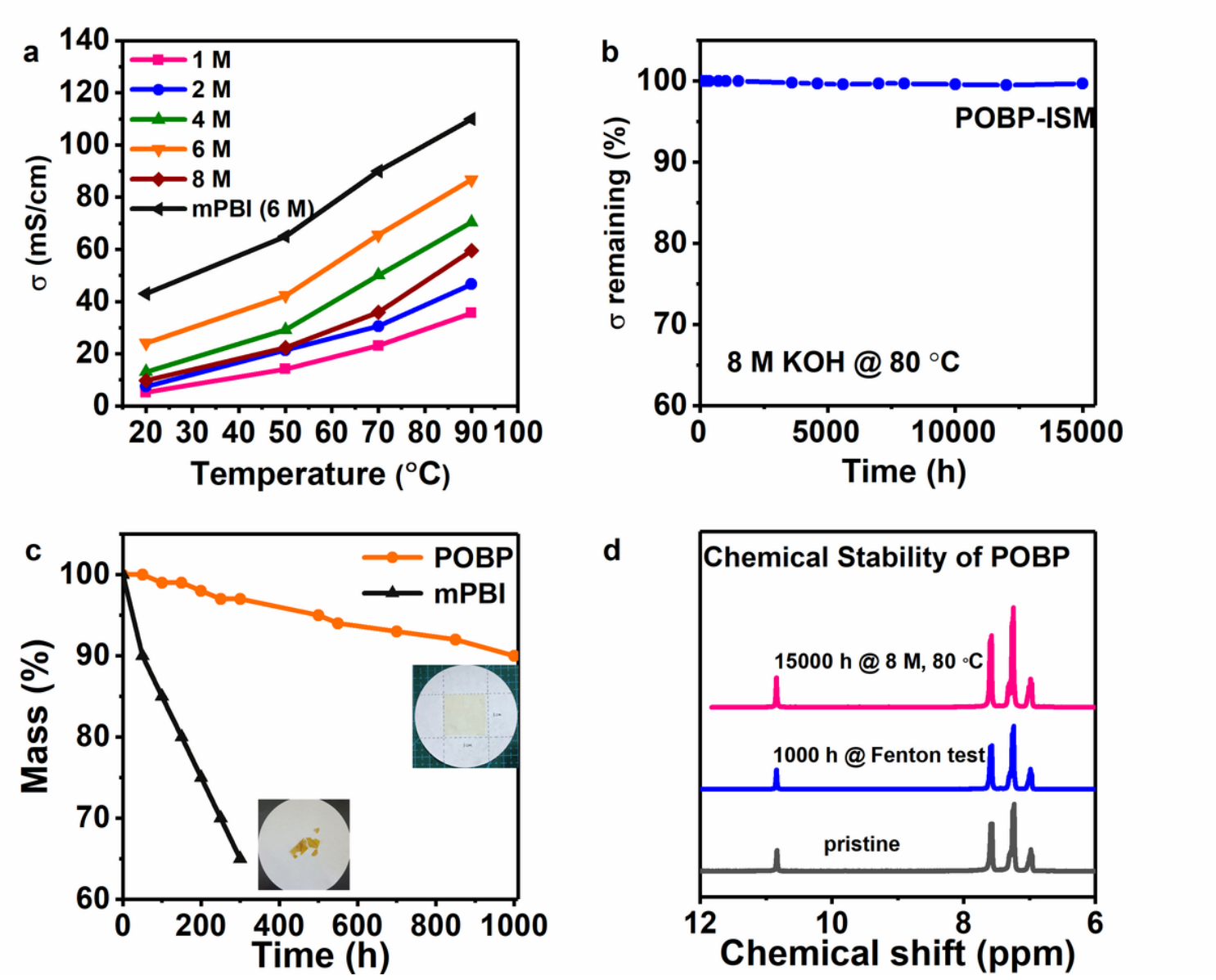

Figure 3

Properties and stability of POBP-ISMs. a, Hydroxide conductivity of membranes the function of KOH concentration and temperature. **b,** Hydroxide conductivity remaining of membrane during alkaline durability testing (8 M KOH at 80°C) over 15000 h. **c,** A comparison of oxidation stability between POBP and mPBI in Fenton test (4ppm at 3 wt% H_2O_2 at 80°C). **d,** ^{1}H NMR spectrums of pristine and aged POBP after alkaline during the test and Fenton test.

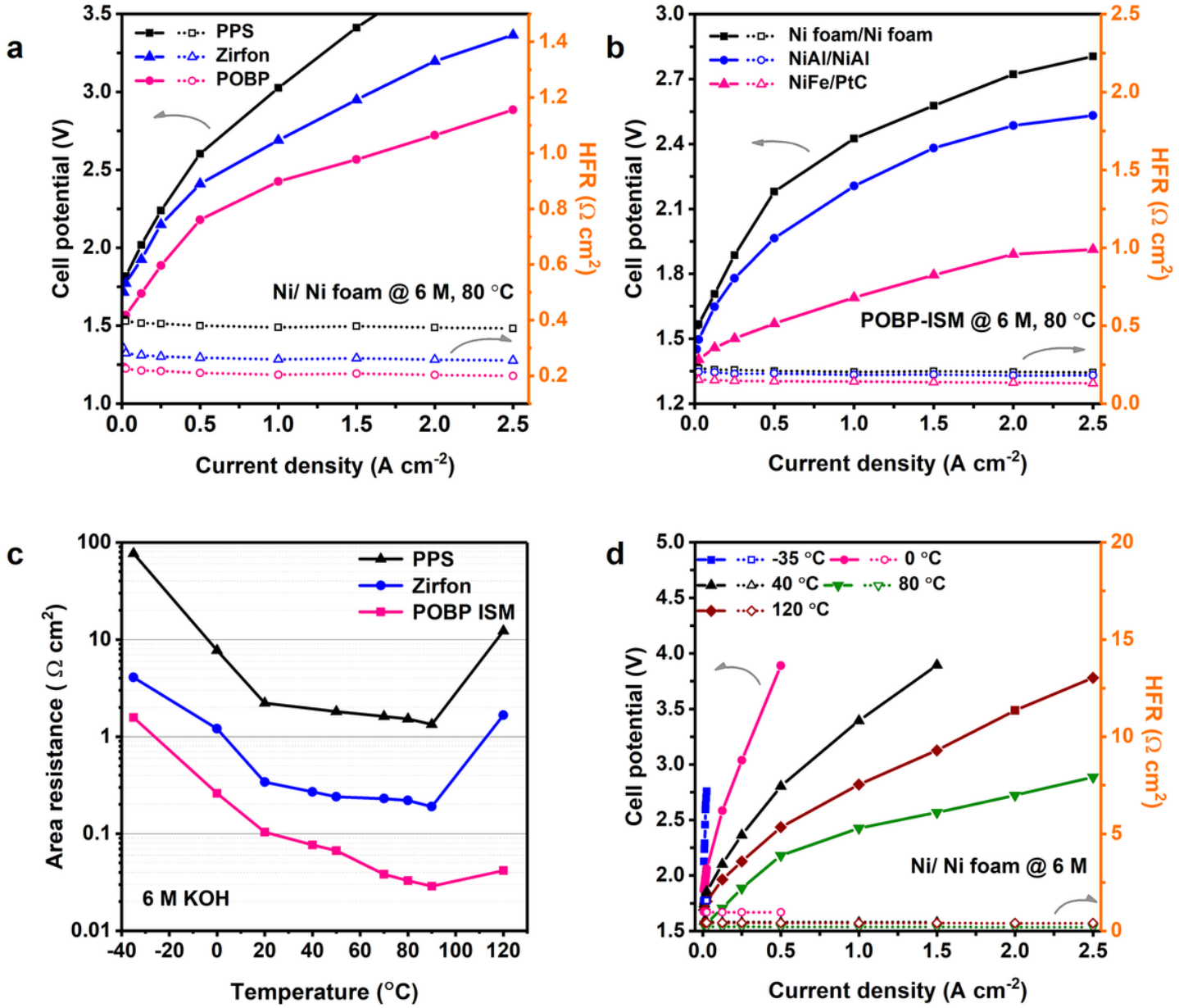

Figure 4

Polarization curves of AWE. **a,** comparison of electrolysis polarization and high-frequency resistance (HFR) consisting of different membranes: Zirfon, POBP-ISM and PPS diaphragm. **b,** the electrolysis polarization consisting of different electrode catalysts with POBP ISMs at 80 °C. **c,** comparison of area resistance (AR) at -35-120 °C of different membranes: Zirfon, POBP-ISM, and PPS diaphragm. **d,** polarization characteristics of POBP ISMs-based electrolysis with Ni foam as catalysts as a function of operating temperature: -35-120 °C.

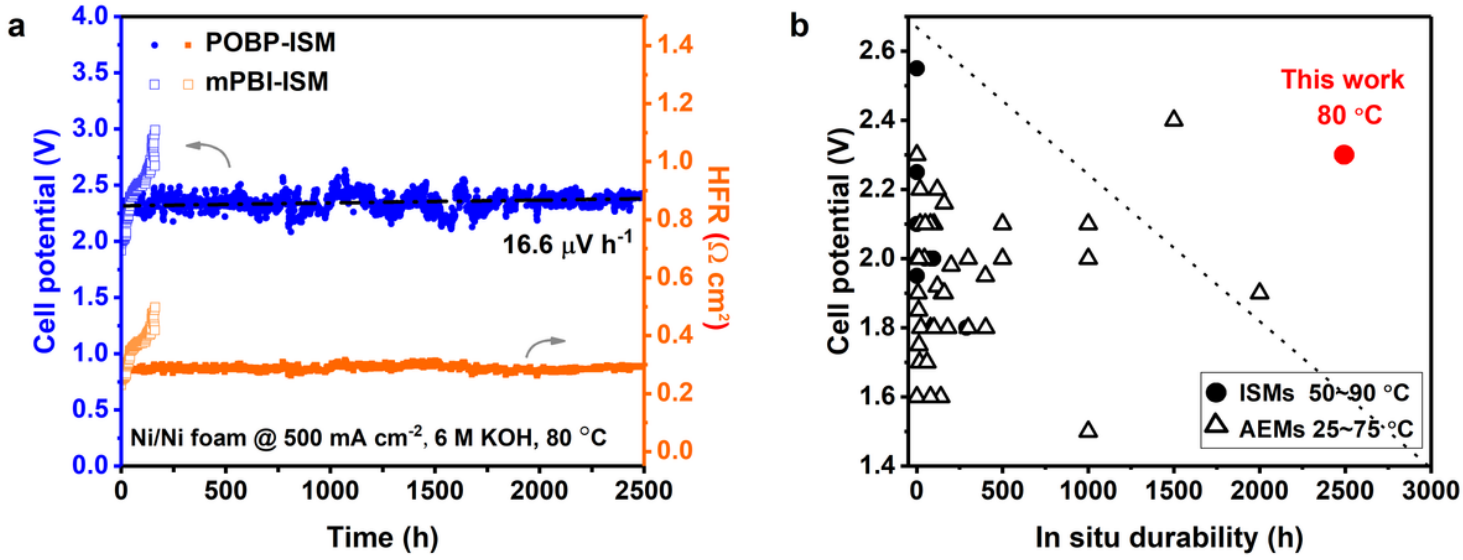

Figure 5

Durability performance of POBP ISM-based AWE. **a,** the in-situ durability of electrolyzer consisting of Ni foam with POBP ISMs at 80°C.Solid blue circles are cell voltage durability of POBP-ISM, solid orange circles are corresponding HFR of POBP-ISM, hollow blue square is cell voltage durability of mPBI-ISM and hollow orange square is the corresponding HFR of mPBI-ISM. **b,** comparison of in-situ durability and cell voltage of present POBP-ISM and current ISMs and AEMs. Red dot symbols denote the present work based on POBP-ISMs, hollow black triangle symbols are reported AEMs[3,6,10,11,17,38-50], and solid black circles are ISMs[22,25,26,51,52].

Supplementary Files

This is a list of supplementary files associated with this preprint. Click to download.

- Supportinginformantion.docx